

Supplementary Materials for “The benefits of ambitious short-term targets when decarbonising the coupled electricity and heating energy system in Europe”

1. Historical greenhouse gases emissions in the European Union

The carbon budget from now onwards for the generation of electricity and the supply of heating in residential and services sector in Europe accounts for 21 GtCO₂. It has been estimated based on a global carbon budget of 800 GtCO₂ to avoid temperature increments above 1.75°C relative to preindustrial period with a probability of greater than 66% [1]. The global budget is assumed to be split among regions according to a constant per-capita ratio which translates into a 6% share for Europe [2]. Out of the total emissions in Europe, the ratio corresponding to electricity and heating is considered constant and equal to present values. In 2017, electricity generation and heating in the residential and services sector emitted 1.56 GtCO₂ which represents 43.5% of European emissions, [3] and Figure 1 .

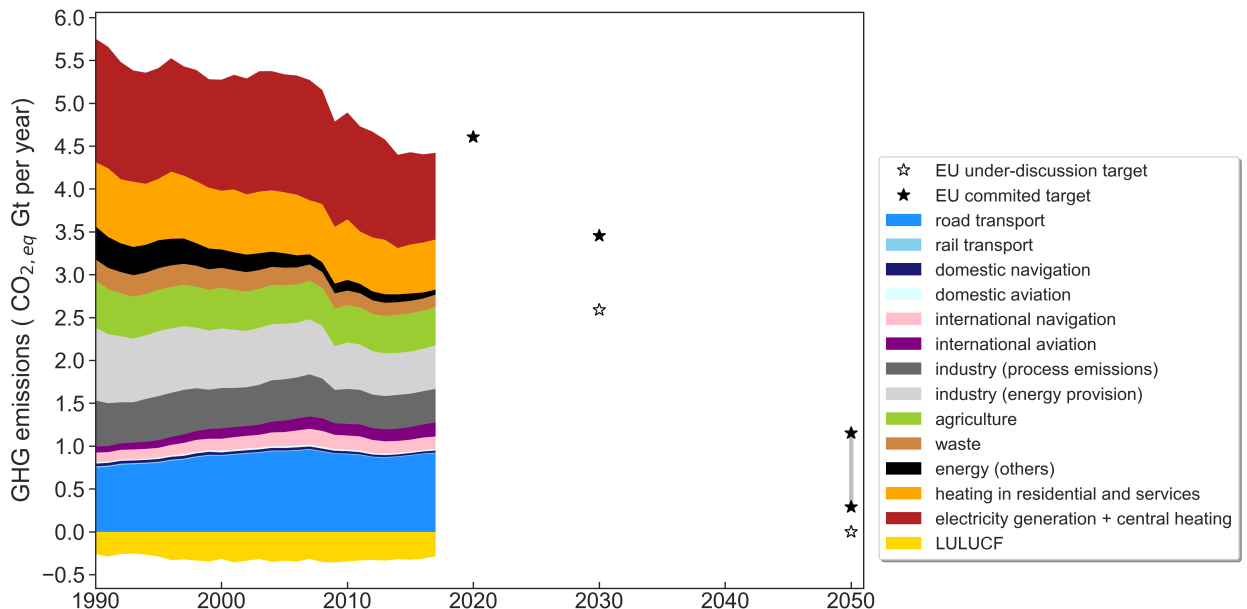


Figure 1: Sectoral distribution of historical emissions in the European Union [3]. The black stars indicate committed EU reduction targets, while white stars mark under-discussion target.

2. CO₂ restriction paths with equivalent budget

The $B=21$ GtCO₂ budget can be utilised following different transition paths. One option consists in assuming a linear CO₂ restriction path. Emissions will then reach zero in t_f

$$t_f = t_0 + \frac{2B}{e_0} \quad (1)$$

where $t_0=2020$, and e_0 represents the carbon emissions from electricity and heating sector in 2020, which are assumed to be the same as in 2017.

Alternatively, emissions can be assumed to follow a path defined by one minus the cumulative distribution function (CDF_β) of a beta distribution in which $\beta_1 = \beta_2$.

$$\begin{aligned} e(t) &= e_0(1 - CDF_\beta(t)) \\ CDF_\beta(t) &= \int_{-\infty}^t PDF_\beta(t)dt \\ PDF_\beta(t) &= \frac{\Gamma(\beta_1 + \beta_2)}{\Gamma(\beta_1) + \Gamma(\beta_2)} t^{\beta_1-1} (1-t)^{\beta_2-1} \end{aligned} \quad (2)$$

where Γ is the gamma function. The cumulative emissions fulfil $\int_{t_0}^{\infty} e(t)dt = B$.

The third option considered for the transition path is an exponential decay, following Raupach *et al.* [2]. In that case, emissions evolve as:

$$e(t) = e_0(1 + (r + m)t)e^{-mt} \quad (3)$$

where r is the initial linear growth rate, which here is assumed to be $r=0$, and the decay parameter m is determined by imposing the integral of the path to be equal to the budget.

$$\begin{aligned} B &= \int_{t_0}^{\infty} e_0(1 + (r + m)t)e^{-mt}dt \\ m &= \frac{1 + \sqrt{1 + \frac{rB}{e_0}}}{\frac{B}{e_0}} \end{aligned} \quad (4)$$

Although the exponential decay path approaches asymptotically to zero, we assume here that $e(2050) = 0$. By doing that, the final point of the different transition paths is equivalent and all of them achieve net-zero emissions by 2050.

3. Historical evolution of CO₂ emissions from heating supply in residential and services sector in European countries

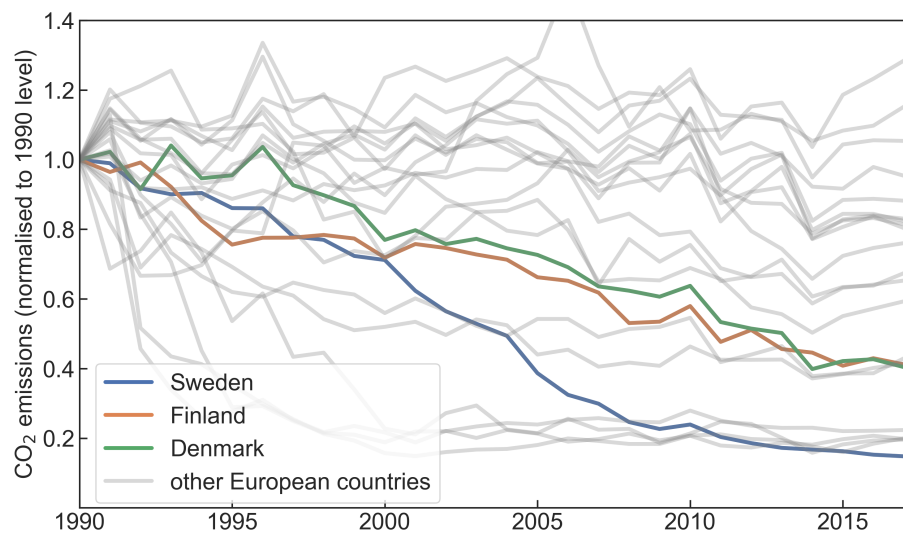


Figure 2: Historical CO₂ emissions from heating in residential and services sector [3].

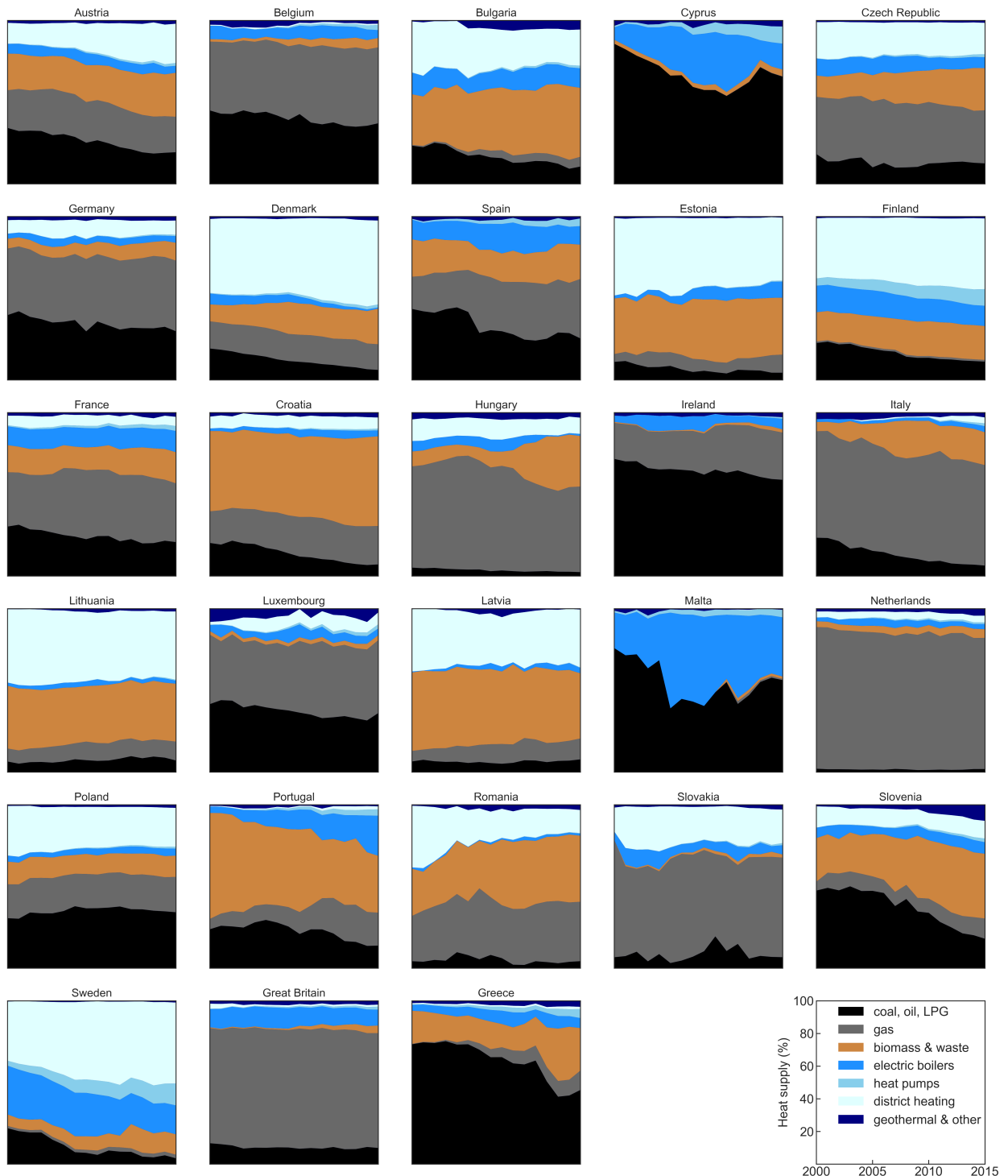


Figure 3: Historical share of technologies used to supply heating demand in residential and services sector [4].

4. Historical build rates for solar photovoltaics in European countries

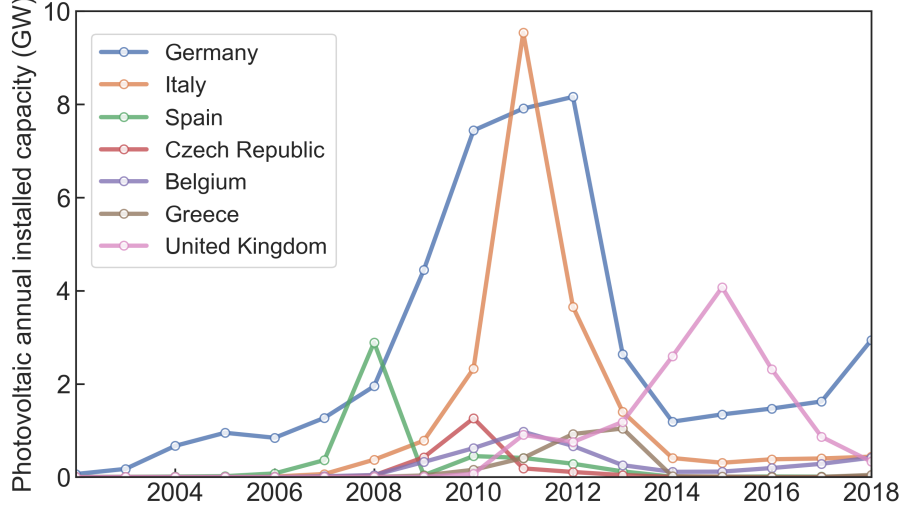


Figure 4: Photovoltaic annual build rates for those European countries with a prominent peak [5]. The sharp increase and subsequent decrease in the installation rates were caused by country-specific successive changes in the regulatory frameworks. See for instance [6, 7].

5. Transition paths cautious and last-minute. Additional results

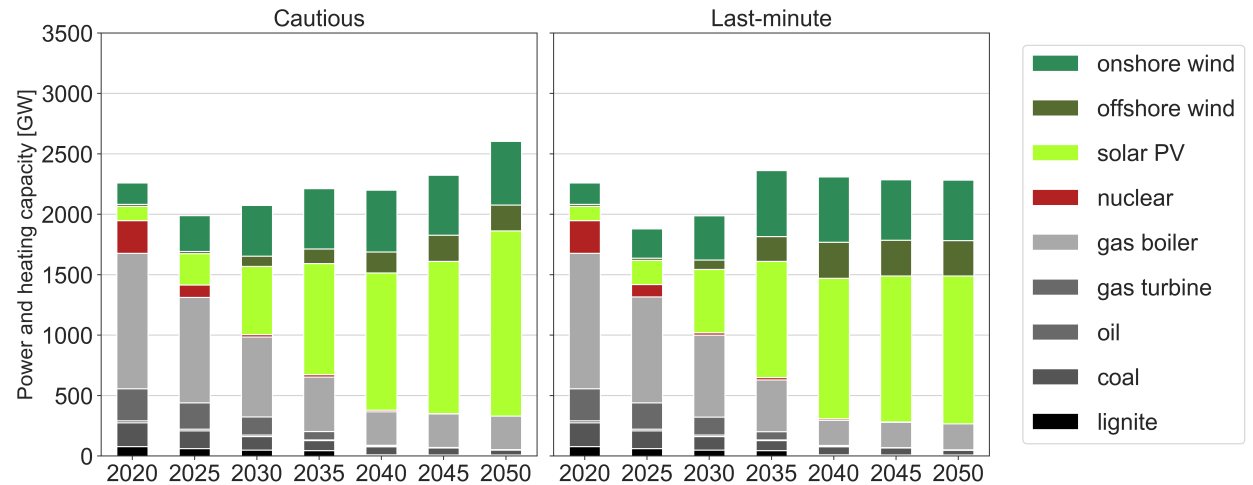


Figure 5: Installed capacities for different technologies throughout transition paths shown in Fig. 1 in the main text.

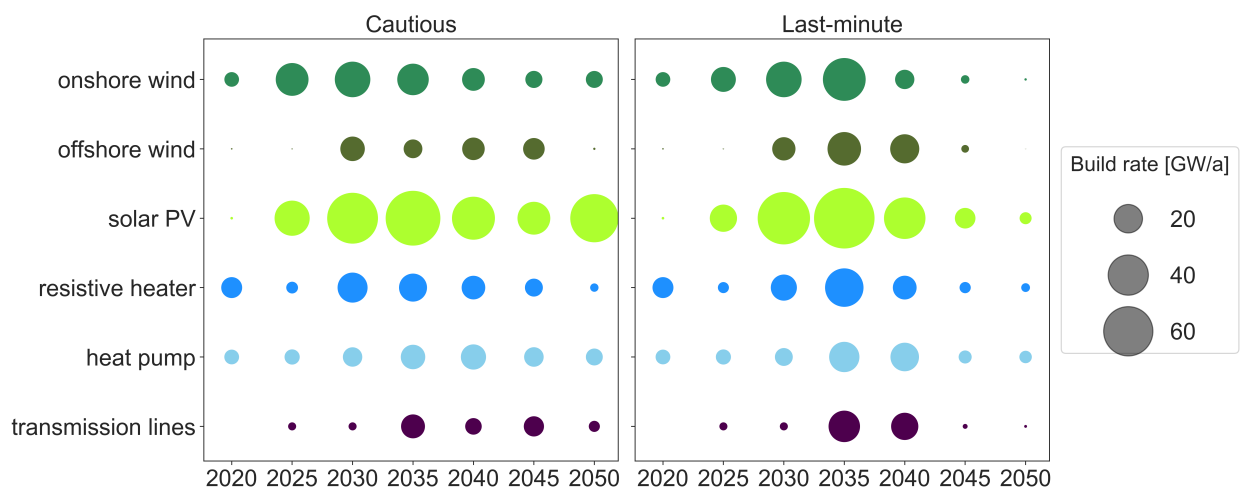


Figure 6: Annual build rates for different technologies throughout transition paths shown in Fig. 1 in the main text.

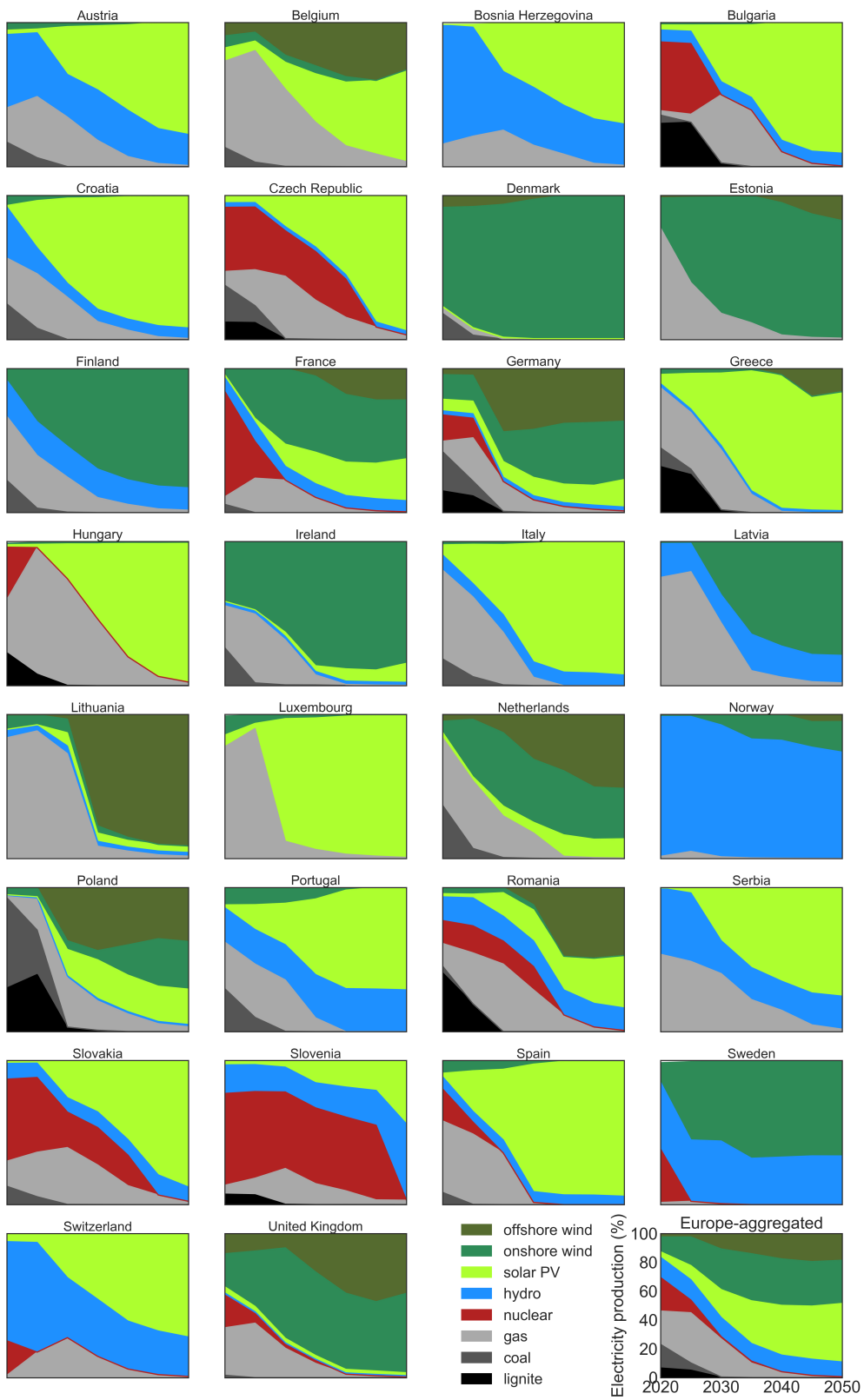


Figure 7: Evolution of electricity generation mix in every country for the Tortoise transition path.

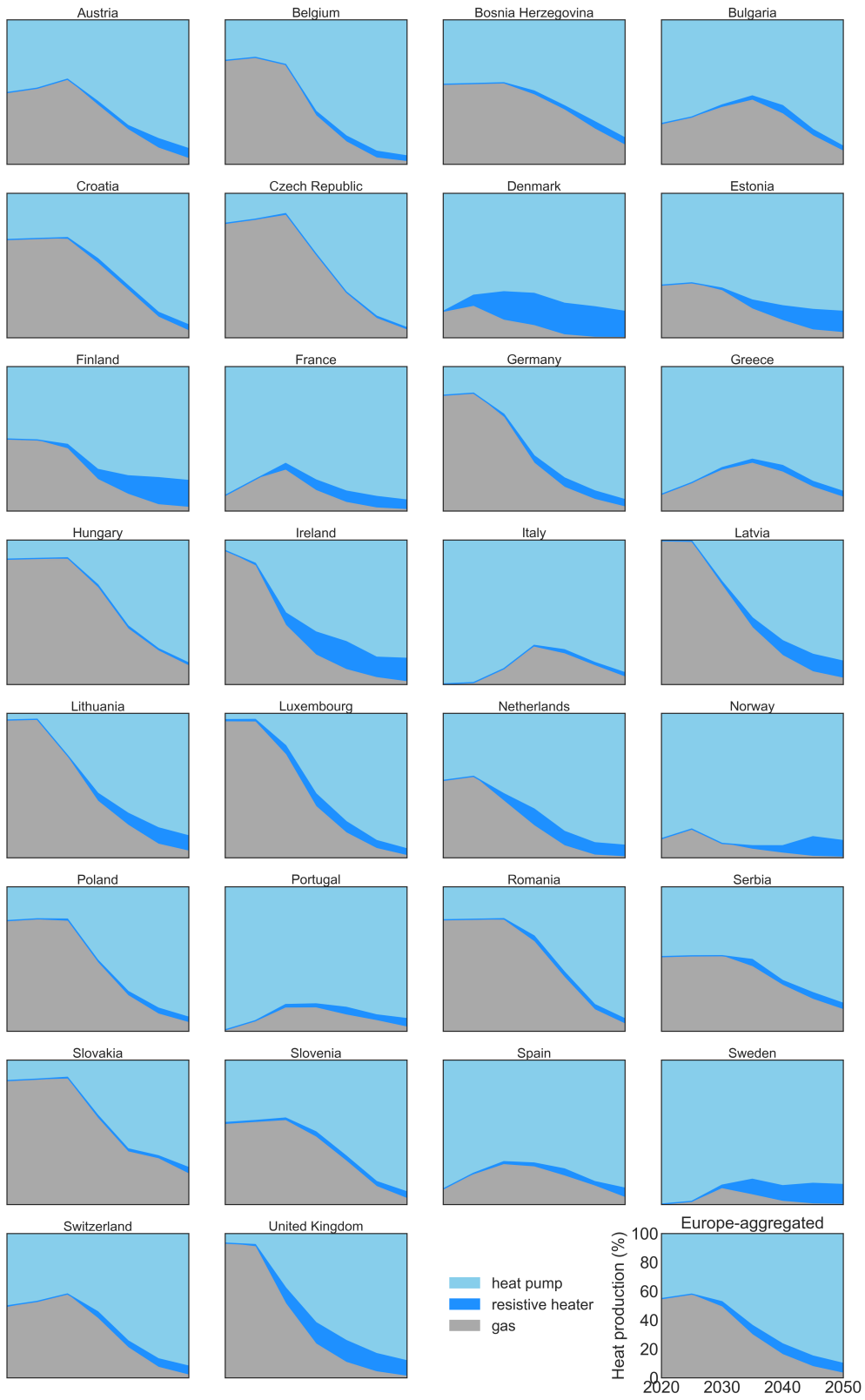


Figure 8: Evolution of technologies used to supply heating in residential and services sector in the cautious path.

6. Model description

In every time step, the optimisation objective, that is, the total annualised system cost is calculated as:

$$\begin{aligned} \min_{\substack{G_{n,s}, E_{n,s}, \\ F_\ell, g_{n,s,t}}} & \left[\sum_{n,s} c_{n,s} \cdot G_{n,s} + \sum_{n,s} \hat{c}_{n,s} \cdot E_{n,s} \right. \\ & \left. + \sum_\ell c_\ell \cdot F_\ell + \sum_{n,s,t} o_{n,s,t} \cdot g_{n,s,t} \right] \end{aligned} \quad (5)$$

where $c_{n,s}$ are the fixed annualised costs for generator and storage power capacity $G_{n,s}$ of technology s in every bus n , $\hat{c}_{n,s}$ are the fixed annualised costs for storage energy capacity $E_{n,s}$, c_ℓ are the fixed annualised costs for bus connectors F_ℓ , and $o_{n,s,t}$ are the variable costs (which in some cases include CO₂ tax), for generation and storage dispatch $g_{n,s,t}$ in every hour t . Bus connectors ℓ include transmission lines but also converters between the buses implemented in every country (see Figure ??), for instance, heat pumps that connect the electricity and heating bus.

The optimisation of the system is subject to several constraints. First, hourly demand $d_{n,t}$ in every bus n must be supplied by generators in that bus or imported from other buses. $f_{\ell,t}$ represents the energy flow on the link ℓ and $\alpha_{n,\ell,t}$ indicates both the direction and the efficiency of flow on the bus connectors. $\alpha_{n,\ell,t}$ can be time dependent such as in the case of heat pumps whose conversion efficiency depends on the ambient temperature.

$$\sum_s g_{n,s,t} + \sum_\ell \alpha_{n,\ell,t} \cdot f_{\ell,t} = d_{n,t} \leftrightarrow \lambda_{n,t} \quad \forall n, t \quad (6)$$

The Lagrange multiplier $\lambda_{n,t}$, also known as Karun-Kush-Tucker (KKT), associated with the demand constraint indicates the marginal price of the energy carrier in the bus n , *e.g.*, local marginal electricity price in the electricity bus.

Second, the maximum power flowing through the links is limited by their maximum physical capacity F_ℓ . For transmission links, $\underline{f}_{\ell,t} = -1$ and $\bar{f}_{\ell,t} = 1$, which allows both import and export between neighbouring countries. For a unidirectional converter *e.g.*, a heat resistor, $\underline{f}_{\ell,t} = 0$ and $\bar{f}_{\ell,t} = 1$ since a heat resistor can only convert electricity into heat.

$$\underline{f}_{\ell,t} \cdot F_\ell \leq f_{\ell,t} \leq \bar{f}_{\ell,t} \cdot F_\ell \quad \forall \ell, t. \quad (7)$$

For interconnecting transmission lines, the lengths l_ℓ are set by the distance between the geographical mid-points of each country, so that some of the transmission within each country is also reflected in the optimisation. A factor of 25% is added to the line lengths to account for the fact that transmission lines cannot be placed as the crow flies due to land use restriction. For the transmission lines capacities F_ℓ , a safety margin of 33% of the installed capacity is used to satisfy n-1 requirements [8].

Third, for every hour the maximum capacity that can provide a generator or storage is bounded by the product between installed capacity $G_{n,s}$ and availabilities $\underline{g}_{n,s,t}$, $\bar{g}_{n,s,t}$. For instance, for solar generators $\underline{g}_{n,s,t}$ is zero and $\bar{g}_{n,s,t}$ refers to the capacity factor at time t

$$\underline{g}_{n,s,t} \cdot G_{n,s} \leq g_{n,s,t} \leq \bar{g}_{n,s,t} \cdot G_{n,s} \quad \forall n, s, t. \quad (8)$$

The maximum power capacity for generators is limited by potentials $\bar{G}_{n,s}$ that are estimated taking into account physical and environmental constraints:

$$0 \leq G_{n,s} \leq \bar{G}_{n,s} \quad \forall n, s. \quad (9)$$

The storage technologies have a charging efficiency η_{in} and rate $g_{n,s,t}^+$, a discharging efficiency η_{out} and rate $g_{n,s,t}^-$, possible inflow $g_{n,s,t,inflow}$ and spillage $g_{n,s,t,spillage}$, and standing loss η_0 . The state of charge $e_{n,s,t}$ of every storage has to be consistent with charging and discharging in every hour and is limited by the energy capacity of the storage $E_{n,s}$. It should be remarked that the storage energy capacity $E_{n,s}$ can be optimised independently of the storage power capacity $G_{n,s}$.

$$\begin{aligned} e_{n,s,t} = & \eta_0 \cdot e_{n,s,t-1} + \eta_{in}|g_{n,s,t}^+| - \eta_{out}^{-1}|g_{n,s,t}^-| \\ & + g_{n,s,t,inflow} - g_{n,s,t,spillage}, \\ & 0 \leq e_{n,s,t} \leq E_{n,s} \quad \forall n, s, t. \end{aligned} \quad (10)$$

So far, equations (6) to (10) represent mainly technical constraints but additional constraints can be imposed to bound the solution.

The interconnecting transmission expansion can be limited by a global constraint

$$\sum_{\ell} l_{\ell} \cdot F_{\ell} \leq \text{CAP}_{LV} \quad \leftrightarrow \quad \mu_{LV}, \quad (11)$$

where the sum of transmission capacities F_{ℓ} multiplied by the lengths l_{ℓ} is bounded by a transmission volume cap CAP_{LV} . In this case, the Lagrange/KKT multiplier μ_{LV} represents the shadow price of a marginal increase in transmission volume.

The maximum CO₂ allowed to be emitted by the system CAP_{CO2} can be imposed through the constraint

$$\sum_{n,s,t} \varepsilon_s \frac{g_{n,s,t}}{\eta_{n,s}} + \sum_{n,s} \varepsilon_s (e_{n,s,t=0} - e_{n,s,t=T}) \leq \text{CAP}_{CO2} \quad \leftrightarrow \quad \mu_{CO2} \quad (12)$$

where ε_s represents the specific emissions in CO₂-tonne-per-MWh_{th} of the fuel s , $\eta_{n,s}$ the efficiency and $g_{n,s,t}$ the generators dispatch. In this case, the Lagrange/KKT multiplier represents the shadow price of CO₂, *i.e.*, the additional price that should be added for every unit of CO₂ to achieve the CO₂ reduction target in an open market.

7. Sectors description and data

TODO: Add figure with the sectors included.

7.1. Electricity sector

Hourly electricity demand for every country corresponding to 2015 is retrieved from EU Network Transmission System Operators of Electricity (ENTSO-E) via the convenient dataset prepared by the Open Power System Data (OPSD) initiative [9]. In every country, electricity can be generated by solar PV, onshore wind, offshore wind, Open Cycle Gas Turbines (OCGT), Combined Cycle Gas Turbines (CCGT), coal, lignite, and nuclear power plants and CHP units using either gas, coal or biomass. Their costs, lifetimes and efficiencies are shown in Table 4. Country-wise onshore and offshore wind capacity factor time series are modeled by converting wind velocity from Climate Forecast System Reanalysis (CFSR) [10] into wind generation, following the methodology described in [11]. CFSR database comprises hourly resolution and spatial resolution equal to 0.3125°x0.3125°, which in Europe roughly corresponds to 40x40 km². For every country, a capacity layout proportional to wind resource is assumed. Following [12], large countries are divided into up to 4 regions sorted by wind resource. Independent classes of generators with different time series and average full load hours are added to a single node representing a country. Their optimised capacities are later aggregated on a country level for analysis. Time series representing the hourly capacity factors for solar PV were obtained by converting bias-corrected CFSR reanalysis irradiance into solar electricity generation, assuming

Table 1: Land types considered suitable for every technology [14?].

Solar PV	Onshore wind	Offshore Wind
----------	--------------	---------------

a uniform capacity layout across every country. Details on the conversion and aggregation methodology can be found in [13], the complete time series dataset is available in [10.5281/zenodo.1321809](https://doi.org/10.5281/zenodo.1321809). The maximum capacity for onshore wind, offshore wind, and solar PV that can be installed in every country is limited by the estimated potentials. Those are determined by summing the available land in every reanalysis gridcell, which in turn is calculated by considering only the suitable land for every technology, according to the Corine Land Cover database [14] and subtracting Natura 2000 protected areas [15]. For onshore and offshore wind, the potential is calculated as 20% of the available land. For solar PV, 3% of the available land is used for estimating the potential.

$$Potential_{n,PV} = \sum_i 0.03 \cdot A_i^{CLC,PV} (1 - A_i^{Natura2000}) \quad (13)$$

where $A_i^{CLC,PV}$ is the area of the gridcell belonging to PV categories in the Corine Land Cover database, Table 1, and $A_i^{Natura2000}$ is the area of the grid cell protected by Natura 2000 network.

$$Potential_{n,wind} = \sum_i 0.2 \cdot A_i^{CLC,wind} (1 - A_i^{Natura2000}) k_n \quad (14)$$

For wind, k_n is a coefficient calculated by imposing the condition that in none of the grid cells the install capacity surpasses the potential. This represents a conservative approach. Higher potential could be attained if capacity layout is not proportional to the wind resource.

CHP units are modeled as extraction condensing units, the feasible space representing the possible combinations of power and heat outputs is included as a constraint in the model, as detailed in [16]. Electricity can be stored in static batteries and hydrogen storage. Alkaline electrolyzers are assumed since they have a lower cost [17] and higher cumulative installed capacity [18] than PEM electrolyzers. Hydrogen can be stored in overground steel tanks or underground salt caverns [18]. For the latter, energy capacities in every country are limited to the potential estimation for onshore salt caverns within 50 km of shore to avoid environmental issues associated with brine solution disposal, see Figure 7 in [19]. Electricity can also be used to produce methane by combining hydrogen and direct air captured (DAC) CO₂ in the Sabatier reaction. Following [16], the energy consumed in DAC is taken into account by reducing the efficiency of the Sabatier reaction to 60%. Alternative CO₂ sources such capturing industry process emissions or biomass-related emissions are not included.

The transmission links between countries are assumed to be high-voltage direct current (HVDC) connections. The lengths l_ℓ are set by the distance between the geographical mid-points of each country, so that some of the transmission within each country is also reflected in the optimisation. A factor of 25% is added to the line lengths to account for the fact that transmission lines cannot be placed as the crow flies due to land use restriction. For the transmission lines capacities F_ℓ , a safety margin of 33% of the installed capacity is used to satisfy n-1 requirements [8]. For 2020 and 2030, the capacities correspond to the values assumed in the ENTSOE Ten-Year Network Development Plan (TNYDP), see Table 2 and [20]. The values for 2025 are interpolated assuming a linear capacity expansion between 2020 and 2030 for every link. For years from 2035 onwards, capacities are optimized together with the rest of the system components using 2030 values as the lower boundary. This is true for all the analyses except when we look at constrained capacity expansion by keeping the capacities of transmission links fixed after 2030.

7.2. Heating sector

Annual heat demands for European countries are retrieved from [21]. They are converted into hourly heat demand based on the population-weighted [22] Heating Degree Hour (HDH), that is, heating is assumed to be proportional to the difference between ambient temperature and a threshold temperature. 17°C is assumed

Table 2: Transmission capacities (MW) for interconnections [20].

Link	2020	2030	Link	2020	2030	Link	2020	2030
AL-GR	250	250	FI-EE	1000	1000	LU-FR	0	0
AL-ME	350	350	FI-NO	0	0	LV-EE	1600	1600
AL-MK	200	200	FI-SE	2300	2800	LV-LT	1200	1800
AL-RS	760	760	FR-BE	4300	4300	ME-AL	350	350
AT-CH	1700	1700	FR-CH	3700	3700	ME-BA	400	400
AT-CZ	1000	1000	FR-DE	3000	4800	ME-IT	1200	1200
AT-DE	5000	7500	FR-ES	5000	8000	ME-RS	1000	1000
AT-HU	1200	1200	FR-GB	5400	5400	MK-AL	200	200
AT-IT	555	1655	FR-IE	0	700	MK-BG	150	150
AT-SI	1200	1200	FR-IT	4350	4350	MK-GR	400	400
BA-HR	1344	1844	FR-LU	380	380	MK-RS	1050	1050
BA-ME	500	500	GB-BE	1000	1000	NI-GB	80	500
BA-RS	1100	1100	GB-DK	1400	1400	NI-IE	1100	1100
BE-DE	1000	1000	GB-FR	5400	5400	NL-BE	2400	2400
BE-FR	2800	2800	GB-IE	500	500	NL-DE	4450	5000
BE-GB	1000	1000	GB-IS	0	0	NL-DK	700	700
BE-LU	1080	1080	GB-NI	500	500	NL-GB	1000	1000
BE-NL	2400	2400	GB-NL	1000	1000	NL-NO	700	700
BG-GR	1728	1728	GB-NO	1400	1400	NO-DE	1400	1400
BG-MK	530	530	GR-AL	250	250	NO-DK	1640	1640
BG-RO	1400	1400	GR-BG	1032	1032	NO-FI	0	0
BG-RS	600	600	GR-CY	2000	2000	NO-GB	1400	1400
CH-AT	1700	1700	GR-IT	500	500	NO-NL	700	700
CH-DE	4700	4700	GR-MK	350	350	NO-SE	3695	3695
CH-FR	1300	1300	HR-BA	1312	1812	PL-CZ	600	600
CH-IT	6240	6240	HR-HU	2000	2000	PL-DE	3000	3000
CY-GR	2000	2000	HR-IT	0	0	PL-DK	0	0
CZ-AT	1200	1200	HR-RS	600	600	PL-LT	1000	1000
CZ-DE	2100	2600	HR-SI	2000	2000	PL-PL	5000	5000
CZ-PL	500	500	HU-AT	800	800	PL-SE	600	600
CZ-SK	2100	2100	HU-HR	2000	2000	PL-SK	990	990
DE-AT	5000	7500	HU-RO	1300	1300	PT-ES	3500	3500
DE-BE	1000	1000	HU-RS	600	600	RO-BG	1500	1500
DE-CH	3286	3286	HU-SI	1700	1700	RO-HU	1400	1400
DE-CZ	1500	2000	HU-SK	2000	2000	RO-RS	1450	1450
DE-DK	4000	4000	IE-FR	0	700	RS-AL	330	330
DE-FR	3000	4800	IE-GB	500	500	RS-BA	1200	1200
DE-LU	2300	2300	IE-NI	1100	1100	RS-BG	350	350
DE-NL	4450	5000	IS-GB	0	0	RS-HR	600	600
DE-NO	1400	1400	IT-AT	385	1385	RS-HU	600	600
DE-PL	2000	2000	IT-CH	3860	3860	RS-ME	1100	1100
DE-SE	615	1315	IT-FR	2160	2160	RS-MK	950	950
DK-DE	4000	4000	IT-GR	500	500	RS-RO	1050	1050
DK-DK	1200	1200	IT-HR	0	0	SE-DE	615	1315
DK-GB	1400	1400	IT-IT	5750	5750	SE-DK	1980	1980
DK-NL	700	700	IT-ME	1200	1200	SE-FI	2400	3200
DK-NO	1640	1640	IT-SI	1380	1380	SE-LT	700	700
DK-PL	0	0	IT-TN	0	0	SE-NO	3995	3995
DK-SE	2440	2440	LT-LV	1500	2100	SE-PL	600	600
EE-FI	1016	1016	LT-PL	1000	1000	SI-AT	1200	1200
EE-LV	1600	1600	LT-SE	12700	700	SI-HR	2000	2000
ES-FR	5000	8000	LU-BE	700	700	SI-HU	2000	2000
ES-PT	4200	4200	LU-DE	2300	2300	SI-IT	1530	1530

as threshold temperature. Ambient temperature is read from the same reanalysis database [10] used to model wind and solar PV time series. **TODO: Change to daily profiles?** For every country, heating demand is split between low-population density areas and high-population density areas. 44.6% of the European population is estimated to live in the latter [16] where district heating systems can be deployed. In high-density population areas, heating can be supplied by central ground-sourced heat pumps, heat resistors and gas boilers, as well as by CPH units. All the previous technologies are assumed to be integrated in district heating networks. Furthermore, individual air-sourced heat pumps are also allowed in those areas. In low-density population areas, heating can be supplied by individual ground-sourced heat pumps, heat resistors and gas boilers. Costs, lifetimes, and efficiencies of the different technologies are included in Table 4.

The Coefficient of Performance (COP) of heat-pumps depends on ambient or ground temperature to capture the lower COP in winter. COP depends on the difference between the source and the sink temperatures $\Delta T = T_{sink} - T_{source}$. For air-sourced heat pumps (ASHP), $COP = 6.81 + 0.121\Delta T + 0.000630\Delta T^2$, for ground-sourced heat pumps (GSHP), $COP = 8.77 + 0.150\Delta T + 0.000734\Delta T^2$ [23]. The sink water temperature is assumed to be $T_{sink} = 55^\circ\text{C}$, the source temperature for air and ground is taken from the same reanalysis database used to estimate heating demand [10]. Thermal energy can be stored in large water pits associated with district heating systems and individual thermal energy storage (TES), *i.e.*, small water tanks. A thermal energy density of 46.8 kWh_{th}/m³ is assumed, corresponding to a temperature difference of 40 K. The decay of thermal energy $1 - \exp(-\frac{1}{24\tau})$ is assumed to have a time constant of $\tau=180$ days for central TES and $\tau=3$ days for individual TES. Charging and discharging efficiencies are 90% due to pipe losses.

Capacities already existing for technologies supplying heat are retrieved from [24]. For the sake of simplicity, coal, oil and gas boilers capacities are assimilated to gas boilers. Besides that, existing capacities for heat resistors, ASHP, GSHP and **biomass** boilers are included in the model. For high-density population areas, the penetration of district-heating is assumed to remain fixed at 2015 values [25] and Table 3.

Describe other scenarios

Cooling demand is currently supplied by electricity so it is included in the electricity demand time series. It is assumed to remain constant throughout the paths. For a thorough discussion of the impact of changing cooling demand, the reader is referred to [26].

7.3. Biomass

The solid biomass can be burnt in CHP or central heating plants associated with district heating systems or in power plants to produce electricity . The model does not include biogas that could be burnt or upgraded into biomethane. A conservative approach is followed to estimate biomass potentials in every country. From the JRC-ENSPRESO database [27, 28], the potential estimations for 2030 in the scenario ‘medium’ are retrieved, but only the types of biomass which are not competing with crops are considered valid. In essence, biomass potentials include only the following items: primary agricultural residues, primary and secondary forestry energy residues including sawdust, forestry residues from landscape care, and municipal waste.

7.3.1. Existing power plants and decommissioning

For conventional technologies, *i.e.* OCGT, CCGT, coal, lignite, nuclear and CHP, installed capacities in every country in 2020 and commissioning dates are retrieved from [29]. A two-step method was implemented to fill commissioning date for power plants whose data was missing. First, for units larger than 50 MW, commissioning dates have been searched and manually added. Then, for smaller units, a Kernel Density Estimation (KDE) approach is used. In essence, for every technology and country, the units with available data are used to create a distribution, which is then used to assign an estimated commissioning date for those units with missing data. For solar PV, the installed capacities in 2020 and the installation dates were obtained by processing annual installed capacities statistics from [5]. For offshore and onshore wind, capacities and age are retrieved from [30].

Table 3: Current penetration of district heating in European countries [25].

Country	District heating penetration
AT	0.14
BA	0.0
BE	0.0
BG	0.16
CH	0.04
CZ	0.4
DE	0.14
DK	0.64
EE	0.52
ES	0.0
FI	0.39
FR	0.06
GB	0.02
GR	0.0
HR	0.07
HU	0.12
IE	0.0
IT	0.03
LT	0.56
LU	0.0
LV	0.3
NL	0.04
NO	0.03
PL	0.41
PT	0.0
RO	0.23
RS	0.27
SE	0.51
SI	0.09
SK	0.54

Existing power plants are assumed to be decommissioned at their corresponding commissioning date plus lifetime (Table 5). When a power plant has been retrofitted, we assume that its operating life is extended by half of its nominal lifetime. For heating capacities, 25% of existing capacities in 2015 are assumed to be decommissioned in every time step after 2020.

7.4. Levelised Cost of Energy (LCOE)

The Levelised Cost of Energy is defined as the total system cost per unit of consumed energy, that is, including supplied electricity and heating demand.

TODO: Describe path of electrification of transport.

8. Cost assumptions

Figure 9: Cost evolution assumed for the different technologies.

Table 4: Cost assumptions per technology and year. All costs are given in real 2015 money.

Technology ¹	Unit	2020	2025	2030	2035	2040	2045	2050	source
Onshore Wind	€/kW _{el}	1118	1077	1035	1006	977	970	963	[17]
Offshore Wind	€/kW _{el}	2128	2031	1934	1871	1808	1792	1777	[17]
Solar PV (utility-scale)	€/kW _{el}	398	326	254	221	188	169	151	[31]
Solar PV (rooftop)	€/kW _{el}	1127	955	784	723	661	600	539	[32]
OCGT	€/kW _{el}	453	444	435	429	423	417	411	[17]
CCGT	€/kW _{el}	880	855	830	822	815	807	800	[17]
Coal power plant	€/kW _{el}	3845	3845	3845	3845	3845	3845	3845	[33]
Lignite	€/kW _{el}	3845	3845	3845	3845	3845	3845	3845	[33]
Nuclear	€/kW _{el}	7940	7940	7940	7940	7940	7940	7940	[33]
Reservoir hydro	€/kW _{el}	2208	2208	2208	2208	2208	2208	2208	[34]
Run of river	€/kW _{el}	3312	3312	3312	3312	3312	3312	3312	[34]
PHS	€/kW _{el}	2208	2208	2208	2208	2208	2208	2208	[34]
Gas CHP	€/kW _{el}	590	575	560	550	540	530	520	[17]
Biomass CHP	€/kW _{el}	3500	3400	3300	3224	3150	3075	3000	[17]
Coal CHP	€/kW _{el}	1900	1880	1860	1841	1822	1803	1783	[17]
Biomass central heat plant	€/kW _{el}	890	865	840	820	800	780	760	[17]
Biomass power plant	€/kW _{el}	3500	3400	3300	3224	3150	3075	3000	[17]
HVDC overhead	€/MWkm	400	400	400	400	400	400	400	[35]
HVDC inverter pair	€/MW	150000	150000	150000	150000	150000	150000	150000	[35]
Battery storage	€/kWh	232	187	142	118	94	84	75	[17]
Battery inverter	€/kW _{el}	270	215	160	130	100	80	60	[17]
Electrolysis	€/kW _{el}	600	575	550	537	525	512	500	[17]
Fuel cell	€/kW _{el}	1300	1200	1100	1025	950	875	800	[17]
H ₂ storage underground	€/kWh	3.0	2.5	2.0	1.8	1.5	1.4	1.2	[17]
H ₂ storage tank	€/kWh	57	50	44	35	27	24	21	[17]
DAC (direct-air capture)	€/(tCO ₂ /a)	250	250	250	250	250	250	250	[36]
Methanation	€/kW _{H₂}	1000	1000	1000	1000	1000	1000	1000	[37]
Central gas boiler	€/kW _{th}	70	65	60	60	60	60	60	[17]
Decentral gas boiler	€/kW _{th}	312	304	296	289	282	275	268	[17]
Central resistive heater	€/kW _{th}	70	65	60	60	60	60	60	[17]
Decentral resistive heater	€/kW _{th}	100	100	100	100	100	100	100	[37]
Central water tank storage	€/kWh	0.6	0.6	0.5	0.5	0.5	0.5	0.5	[17]
Decentral water tank storage	€/kWh	18	18	18	18	18	18	18	□
Decentral air-sourced heat pump	€/kW _{th}	940	894	850	827	804	782	760	[17]
Central ground-sourced heat pump	€/kW _{th}	657	625	592	577	562	547	532	[17]
Decentral ground-sourced heat pump	€/kW _{th}	1500	1450	1400	1349	1299	1250	1200	[17]

¹ Add item.

Table 5: Efficiency, lifetime and FOM cost per technology (values shown corresponds to 2020).

Technology	FOM ^a [%/a]	Lifetime [a]	Efficiency	Source
Onshore Wind	1.3	27		[17]
Offshore Wind	1.9	27		[17]
Solar PV (utility-scale)	3.0	30		[31]
Solar PV (rooftop)	2.0	30		[32]
OCGT	1.8	25	0.42	[17]
CCGT	3.3	25	0.59	[17]
Coal power plant	1.6	40	0.33	[33]
Lignite	1.6	40	0.33	[33]
Nuclear	1.4	40	0.33	[33]
Reservoir hydro	1.0	80	0.9	[34]
Run of river	2.0	80	0.9	[34]
PHS	1.0	80	0.75	[34]
Gas CHP	3.3	25		[17]
Biomass CHP	3.6	25		[17]
Coal CHP	1.6	25	1.0	[17]
Biomass central heat plant	5.8	25	1.0	[17]
Biomass power plant	3.6	25	0.31	[17]
HVDC overhead	2.0	40		[35]
HVDC inverter pair	2.0	40		[35]
Battery storage	0.0	20		[17]
Battery inverter	0.2	20	0.9	[17]
Electrolysis	5.0	25	0.64	[17]
Fuel cell	5.0	10	0.5	[17]
H ₂ storage underground	2.0	100	1.0	[17]
H ₂ storage tank	1.1	25		[17]
DAC (direct-air capture)	4.0	30		[36]
Methanation	3.0	25	0.6	[37]
Central gas boiler	2.8	25	1.0	[17]
Decentral gas boiler	0.1	20	0.97	[17]
Central resistive heater	1.5	20	0.99	[17]
Decentral resistive heater	2.0	20	0.9	[37]
Central water tank storage	0.5	20		[17]
Decentral water tank storage	1.0	20		[17]
Water tank charger/discharger			0.9	[17]
Decentral air-sourced heat pump	0.0	18		[17]
Central ground-sourced heat pump	0.3	25		[17]
Decentral ground-sourced heat pump	0.0	20		[17]

^a Fixed Operation and Maintenance (FOM) costs are given as a percentage of the overnight cost per year.

^b Hydroelectric facilities are not expanded in this model and are considered to be fully amortized.

^c Efficiency for Combined Heat and Power (CHP) plants depends on the electricity/heat output and it is modelled as described in the text.

^d Coefficient of performance (COP) of heat pump is modelled as a function of temperature, as described in the text.

^e Investments in methanation and DAC are not allowed independently, only together as ‘Methanation+DAC’, see text.

^f The costs for distribution infrastructure and building retrofitting are approximate (see text) and they are therefore not optimised or included in the presented total system costs, but calculated retrospectively and analysed in the text.

Table 6: Costs and emissions coefficient of fuels.

Fuel	Cost [€ /MWh _{th}]	Source	Emissions [tCO ₂ /MWh _{th}]	Source
coal	8.2	[38]	0.336	[39]
lignite	2.9	[34]	0.407	[39]
gas	20.1	[38]	0.201	[39]
nuclear	2.6	[33]	0	
solid biomass	25.2	[27, 40]	0	

^a Raw biomass fuel cost is assumed as the middle value of the range provided in the references for different European countries and types of sustainable biomass.

9. References

- [1] Global Warming of 1.5°C, Intergovernmental Panel on Climate Change (IPCC), Tech. rep. (2018). URL <https://www.ipcc.ch/sr15/>
- [2] M. R. Raupach, S. J. Davis, G. P. Peters, R. M. Andrew, J. G. Canadell, P. Ciais, P. Friedlingstein, F. Jotzo, D. P. Vuuren, C. L. Quéré, *Sharing a quota on cumulative carbon emissions*, Nature Climate Change 4 (10) (2014) 873–879. doi:[10.1038/nclimate2384](https://doi.org/10.1038/nclimate2384).
- [3] National emissions reported to the UNFCCC and to the EU Greenhouse Gas Monitoring Mechanism , EEA. URL <https://www.eea.europa.eu/data-and-maps/data/national-emissions-reported-to-the-unfccc-and-to-the-eu-greenhouse-gas>
- [4] L. Mantzos, T. Wiesenthal, N. Matei, S. Tchung-Ming, M. Rzsai, H. P. Russ, A. Soria, *JRC-IDEES: Integrated Database of the European Energy Sector* doi:[10.2760/182725](https://doi.org/10.2760/182725). URL <http://www.sciencedirect.com/science/article/pii/S0360544216310295>
- [5] Renewable Capacity Statistics 2019, IRENA. URL <https://www.irena.org/publications/2019/Mar/Renewable-Capacity-Statistics-2019>
- [6] Photovoltaics Report, Tech. rep., Fraunhofer ISE (2019). URL <https://www.ise.fraunhofer.de/content/dam/ise/de/documents/publications/studies/Photovoltaics-Report.pdf>
- [7] M. Victoria, C. Gallego, I. Anton, G. Sala, *Past, Present and Future of Feed-in Tariffs in Spain: What are their Real Costs?*, 27th European Photovoltaic Solar Energy Conference and Exhibition (2012) 4612–4616 doi:[10.4229/27thEUPVSEC2012-6CV.3.49](https://doi.org/10.4229/27thEUPVSEC2012-6CV.3.49). URL <http://www.eupvsec-proceedings.com/proceedings?paper=17736>
- [8] T. Brown, P. Schierhorn, E. Tröster, T. Ackermann, Optimising the european transmission system for 77% renewable electricity by 2030 10 (1) 3–9. doi:[10.1049/iet-rpg.2015.0135](https://doi.org/10.1049/iet-rpg.2015.0135).
- [9] Open Power System Data. 2018. Data Package Time series. Version 2018-03-13. (Primary data from various sources, for a complete list see URL). URL https://data.open-power-system-data.org/time_series/2018-03-13/.
- [10] S. Saha, S. Moorthi, X. Wu, J. Wang, S. Nadiga, P. Tripp, D. Behringer, Y.-T. Hou, H. Chuang, M. Iredell, M. Ek, J. Meng, R. Yang, M. P. Mendez, H. van den Dool, Q. Zhang, W. Wang, M. Chen, E. Becker, *NCEP climate forecast system version 2 (CFSv2) selected hourly time-series products* (2011). URL <https://doi.org/10.5065/D6N877VB>
- [11] G. B. Andresen, A. A. Søndergaard, M. Greiner, *Validation of Danish wind time series from a new global renewable energy atlas for energy system analysis*, Energy 93 (Part 1) (2015) 1074 – 1088. doi:<https://doi.org/10.1016/j.energy.2015.09.071>. URL <http://www.sciencedirect.com/science/article/pii/S0360544215012815>
- [12] D. P. Schlachtberger, T. Brown, S. Schramm, M. Greiner, *The benefits of cooperation in a highly renewable European electricity network*, Energy 134 (Supplement C) (2017) 469–481. doi:[10.1016/j.energy.2017.06.004](https://doi.org/10.1016/j.energy.2017.06.004). URL <http://www.sciencedirect.com/science/article/pii/S0360544217309969>
- [13] M. Victoria, G. B. Andresen, *Using validated reanalysis data to investigate the impact of the PV system configurations at high penetration levels in european countries*, Progress in Photovoltaics: Research and Applications 27 (7) 576–592. doi:[10.1002/pip.3126](https://doi.org/10.1002/pip.3126). URL <https://onlinelibrary.wiley.com/doi/full/10.1002/pip.3126>
- [14] Corine land cover 2006, Tech. rep., EEA (2014). URL <https://www.eea.europa.eu/data-and-maps/data/clc-2006-raster-4>
- [15] Natura 2000 data - the European network of protected sites. URL <https://www.eea.europa.eu/data-and-maps/data/natura-8>
- [16] T. Brown, D. Schlachtberger, A. Kies, S. Schramm, M. Greiner, *Synergies of sector coupling and transmission reinforcement*

- in a cost-optimised, highly renewable European energy system, Energy 160 (2018) 720–739. doi:10.1016/j.energy.2018.06.222.
 URL <http://www.sciencedirect.com/science/article/pii/S036054421831288X>
- [17] Technology Data for Generation of Electricity and District Heating, update november 2019, Tech. rep., Danish Energy Agency and Energinet.dk (2019).
 URL <https://ens.dk/en/our-services/projections-and-models/technology-data/technology-data-generation-electricity-and-fuel-cells-in-the-global-energy-system>, Energy & Environmental Science 12 (2) (2019) 463–491. doi:10.1039/C8EE01157E.
- [18] I. Staffell, D. Scamman, A. V. Abad, P. Balcombe, P. E. Dodds, P. Ekins, N. Shah, K. R. Ward, The role of hydrogen and fuel cells in the global energy system, Energy & Environmental Science 12 (2) (2019) 463–491. doi:10.1039/C8EE01157E.
 URL <https://pubs.rsc.org/en/content/articlelanding/2019/ee/c8ee01157e>
- [19] D. Caglayan, N. Weber, H. U. Heinrichs, J. Linen, M. Robinius, P. A. Kukla, D. Stolten, Technical Potential of Salt Caverns for Hydrogen Storage in Europe doi:10.20944/preprints201910.0187.v1.
 URL <https://www.preprints.org/manuscript/201910.0187/v1>
- [20] Ten-Year Network Development Plan 2016, ENTSOE.
 URL <https://tyndp.entsoe.eu/maps-data/>
- [21] Deliverable 3.1: Profile of heating and cooling demand in 2015. Data Annex, Heat Roadmap Europe.
 URL www.heatroadmap.eu
- [22] Population density by NUTS 3 region.
 URL <https://data.europa.eu>
- [23] I. Staffell, D. Brett, N. Brandon, A. Hawkes, A review of domestic heat pumps, Energy & Environmental Science 5 (11) 9291–9306. doi:10.1039/C2EE22653G.
 URL <https://pubs.rsc.org/en/content/articlelanding/2012/ee/c2ee22653g>
- [24] Mapping and analyses of the current and future (2020 - 2030) heating/cooling fuel deployment (fossil/renewables).
 URL <https://ec.europa.eu/energy/en/studies/mapping-and-analyses-current-and-future-2020-2030-heatingcooling-fuel-deployment>
- [25] Euro Heat and Power.
 URL <https://www.euroheat.org/knowledge-hub/country-profiles/>
- [26] K. Zhu, M. Victoria, G. B. Andresen, M. Greiner, Impact of climatic, technical and economic uncertainties on the optimal design of a coupled fossil-free electricity, heating and cooling system in Europe, Applied Energy 262 (2020) 114500. doi:10.1016/j.apenergy.2020.114500.
 URL <http://www.sciencedirect.com/science/article/pii/S030626192030012X>
- [27] P. Ruiz, A. Sgobbi, W. Nijs, C. Thiel, F. Dalla, T. Kober, B. Elbersen, G. H. Alterra, The JRC-EU-TIMES model. bioenergy potentials for EU and neighbouring countries.
 URL https://setis.ec.europa.eu/sites/default/files/reports/biomass_potentials_in_europe.pdf
- [28] ENSPRESO Biomass database, JRC.
 URL <https://data.jrc.ec.europa.eu/dataset/74ed5a04-7d74-4807-9eab-b94774309d9f/resource/94aca7d6-89af-4969-a74c-2c7ab4376788>
- [29] powerplantmatching.
 URL <https://github.com/FRESNA/powerplantmatching>
- [30] Wind energy database.
 URL <https://www.thewindpower.net/>
- [31] E. Vartiainen, G. Masson, C. Breyer, D. Moser, E. R. Medina, Impact of weighted average cost of capital, capital expenditure, and other parameters on future utility-scale PV levelised cost of electricity, Progress in Photovoltaics: Research and Applications doi:10.1002/pip.3189.
 URL <https://onlinelibrary.wiley.com/doi/abs/10.1002/pip.3189>
- [32] E. Vartiainen, G. Masson, C. Breyer, The true competitiveness of solar PV: a European case study, Tech. rep., European technology and innovation platform for photovoltaics (2017).
 URL http://www.etip-pv.eu/fileadmin/Documents/ETIP_PV_Publications_2017-2018/LCOE_Report_March_2017.pdf
- [33] Lazard's Levelized Cost of Energy Analysis, version 13.0.
 URL <https://www.lazard.com/media/451086/lazards-levelized-cost-of-energy-version-130-vf.pdf>
- [34] A. Schröeder, F. Kunz, F. Meiss, R. Mendelevitch, C. von Hirschhausen, Current and prospective costs of electricity generation until 2050, Data Documentation, DIW 68. Berlin: Deutsches Institut.
 URL <https://www.econstor.eu/handle/10419/80348>
- [35] S. Hagspiel, C. Jägemann, D. Lindenberger, T. Brown, S. Cherevatskiy, E. Tröster, Cost-optimal power system extension under flow-based market coupling, Energy 66 (2014) 654–666. doi:10.1016/j.energy.2014.01.025.
 URL <http://www.sciencedirect.com/science/article/pii/S0360544214000322>
- [36] M. Fasih, D. Bogdanov, C. Breyer, Long-Term Hydrocarbon Trade Options for the Maghreb Region and EuropeRenewable Energy Based Synthetic Fuels for a Net Zero Emissions World, Sustainability 9 (2) (2017) 306. doi:10.3390/su9020306.
 URL <https://www.mdpi.com/2071-1050/9/2/306>
- [37] K. Schaber, Integration of Variable Renewable Energies in the European power system: a model-based analysis of transmission grid extensions and energy sector coupling, Ph.D. thesis, TU München (2013).
 URL <https://d-nb.info/1058680781/34>
- [38] BP Statistical Review of World Energy.
 URL <https://www.bp.com/content/dam/bp/business-sites/en/global/corporate/pdfs/energy-economics/statistical-review/bp-stats-review-2019-full-report.pdf>
- [39] Development of the specific carbon dioxide emissions of the German electricity mix in the years 1990 - 2018, German Environment Agency.

- URL https://www.umweltbundesamt.de/sites/default/files/medien/1410/publikationen/2019-04-10_cc_10-2019_strommix_2019.pdf
- [40] W. Zappa, M. Junginger, M. van den Broek, Is a 100% renewable European power system feasible by 2050?, Applied Energy 233-234 (2019) 1027–1050. doi:10.1016/j.apenergy.2018.08.109.
URL <http://www.sciencedirect.com/science/article/pii/S0306261918312790>